Published online 31 August 2011 *Nucleic Acids Research, 2011, Vol. 39, No. 22* ***9681–9694***
doi:10.1093/nar/gkr680

Guiding strand passage: DNA-induced movement of the gyrase C-terminal domains defines an early step in the supercoiling cycle

Martin A. Lanz[1] and Dagmar Klostermeier[1,2,*]

[1]University of Basel, Biozentrum, Biophysical Chemistry, Klingelbergstrasse 70, CH-4056 Basel, Switzerland and [2]University of Muenster, Institute for Physical Chemistry, Corrensstrasse 30, D-48149 Muenster, Germany

Received May 24, 2011; Revised and Accepted August 1, 2011

ABSTRACT

DNA gyrase catalyzes ATP-dependent negative supercoiling of DNA in a strand passage mechanism. A double-stranded segment of DNA, the T-segment, is passed through the gap in a transiently cleaved G-segment by coordinated closing and opening of three protein interfaces in gyrase. T-segment capture is thought to be guided by the C-terminal domains of the GyrA subunit of gyrase that wrap DNA around their perimeter and cause a DNA-crossing with a positive handedness. We show here that the C-terminal domains are in a downward-facing orientation in the absence of DNA, but swing up and rotate away from the gyrase body when DNA binds. The upward movement of the C-terminal domains is an early event in the catalytic cycle of gyrase that is triggered by binding of a G-segment, and first contacts of the DNA with the C-terminal domains, and contributes to T-segment capture and subsequent strand passage.

INTRODUCTION

Gyrase is a topoisomerase that introduces negative supercoils into DNA in an ATP-dependent reaction (1). Supercoiling occurs by a strand passage mechanism (2–5). Gyrase cleaves a double-stranded DNA (G-segment) to generate a gap through which a second DNA segment (T-segment) is transported. Directed strand passage requires the coordinated opening and closing of three protein interfaces, the so-called gates. The N-gate is formed by the GyrB subunits that dimerize upon ATP binding, causing N-gate closure (6,7). The DNA-gate is formed by the GyrA and GyrB subunits and is close to the conserved tyrosines that catalyze G-segment cleavage (Figure 1). The C-gate is formed by the GyrA subunits. The T-segment of DNA enters gyrase through the open N-gate and is trapped in the upper cavity upon N-gate closure. After DNA-gate opening and strand passage, the T-segment is expelled from the bottom cavity by DNA-gate closure and C-gate opening.

The mechanism that coordinates opening and closing of individual gates is currently not well understood. We have previously shown that DNA bound at the DNA-gate is distorted in a process coupled to cleavage (8). The distortion may reflect an unlocking of the DNA-gate, preparing it for opening and strand passage once a T-segment has been captured. Negative supercoiling requires the DNA substrate to be wrapped around gyrase in a positive handedness, involving wrapping around the carboxy-terminal domains (CTDs) of GyrA (9–11). Binding of DNA at the DNA-gate and complete wrapping of DNA around the CTDs of gyrase cause a narrowing of the N-gate, preparing the N-gate for complete closure upon ATP binding (12). Possibly, the narrowing of the N-gate is linked to unlocking the DNA-gate. Our results indicate that binding of ATP and N-gate closure poise the supercoiling reaction toward strand passage (12) and point toward an active role of the CTDs in the coordination of gate movements during DNA supercoiling by gyrase.

The structure of a number of gyrase CTDs has been reported (10,11,13), and all of them resemble a β-pinwheel comprised of six blades. The isolated CTD wraps DNA around its perimeter, possibly involving blades 1, 6, 5 and 4 (11), thereby imposing a 180° bend on a 40-bp segment (10). The first blade contains a conserved sequence, the so-called GyrA box (14), that is essential for DNA wrapping by the CTDs, and for DNA supercoiling (15). While a structure of the complete GyrA comprising the CTDs is lacking, the CTD position has been deduced from electron microscopy (16) and SAXS data (17,18). However, the models put forward are not in agreement, and the effect of DNA binding on the position of the CTDs is controversially discussed. Originally, it was concluded from electron micrographs that GyrA adopts an extended conformation, with the CTDs facing away from the dimerization interfaces, and located on the same axis as the catalytic tyrosines (16). A later SAXS

*To whom correspondence should be addressed. Tel: +0049 251 83 23421; Fax: +0049 251 83 29138; Email: dagmar.klostermeier@uni-muenster.de

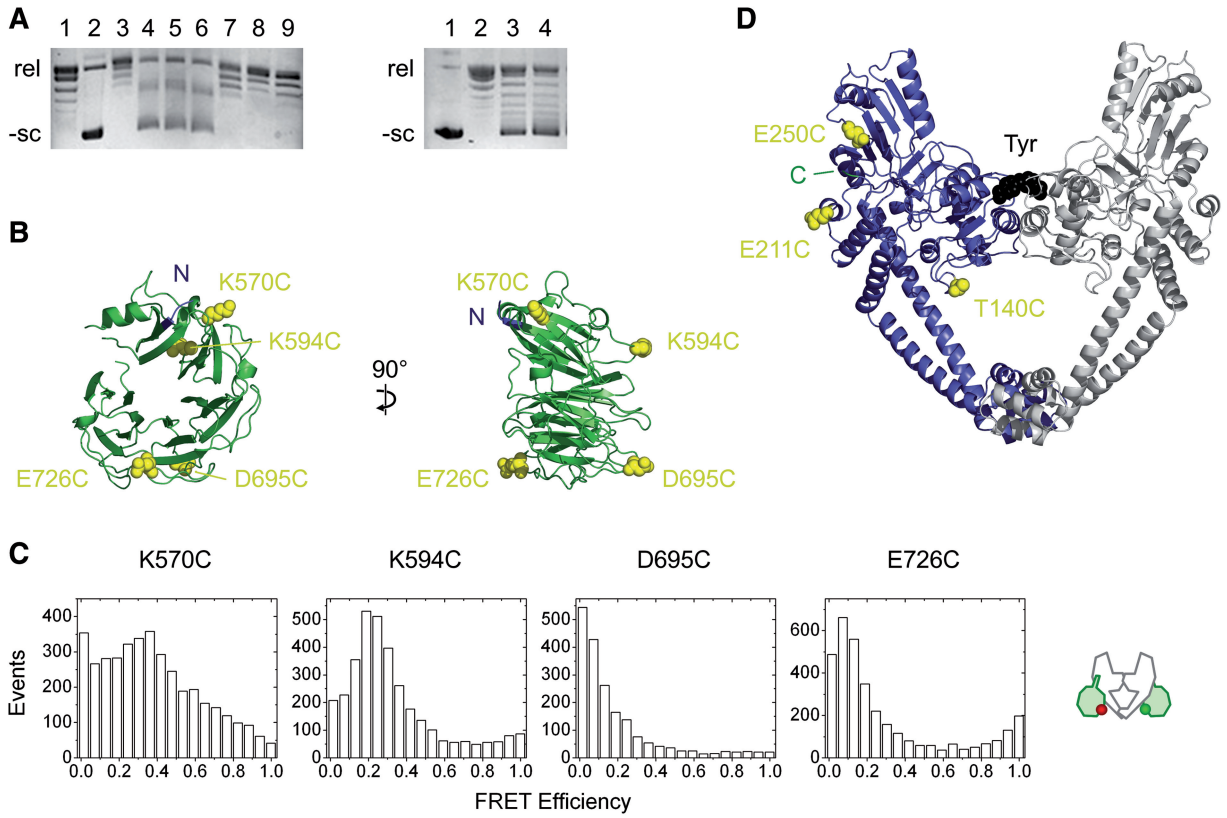

Figure 1. Activity of constructs and positions for fluorophore attachment. (**A**) Left: DNA relaxation by GyrA_ΔCTD. (1) Relaxed plasmid; (2) negatively supercoiled plasmid; (3) relaxation by wild-type gyrase (25 min); (4, 5) after incubation with gyrase lacking the CTDs in the absence of ATP (25 and 80 min); only nicking and formation of linear DNA is observed, but no relaxation occurs; (6–9) relaxation by gyrase lacking the CTDs in the presence of ATP (1, 5, 25, and 80 min); after 1 min, only nicking and formation of linear DNA are observed as in the absence of ATP, but for later time points, the generation of relaxed DNA is evident. Right: DNA supercoiling by gyrase with heterodimeric GyrA. (1) Negatively supercoiled plasmid; (2) relaxed plasmid; (3) supercoiling by wild-type gyrase in the presence of ATP; (4) supercoiling by gyrase containing heterodimeric GyrA containing one cysteine-free subunit and one subunit containing two cysteines (GyrA_T140C_K570C). (**B**) Homology model of the *B. subtilis* CTDs, created with the structure of the *E. coli* GyrA CTDs as a template (see 'Materials and Methods' section). Side chains of residues exchanged to cysteines are shown in yellow. N marks the N-terminus of the CTD. (**C**) smFRET histograms for GyrA homodimers carrying a donor and acceptor fluorophore in both CTDs (see cartoon). (**D**) Structural model of *B. subtilis* GyrA (body), created with the structure of the *E. coli* GyrA as a template (see 'Materials and Methods' section). One monomer is shown in blue and the second in gray. The catalytic tyrosines are depicted in black. The upper dimerization interface close to the tyrosines is called the DNA-gate, the lower dimerization interface is the C-gate. The N-gate is formed by the GyrB subunits (not shown) that bind to the upper part of GyrA. Side chains of residues exchanged to cysteines are shown in yellow. E211 and E250 are located in the tower domain; T140C is close to the DNA-gate. C marks the C-terminus of the GyrA body.

study came to the conclusion that the CTDs are facing downward, and suggested that the CTDs swing up into the extended conformation upon DNA binding and thereby assist in T-segment capture (17). Surprisingly, a recent study of the gyrase/DNA complex also placed the CTDs downward, close to the C-gate (18).

Single-molecule fluorescence resonance energy transfer (smFRET) is ideally suited for mapping global conformations, without limitations for size or complexity. We have used smFRET to map the position of the CTDs with respect to the GyrA body and have monitored conformational changes upon DNA binding, and during DNA supercoiling. Our results demonstrate that the GyrA CTDs are facing downward and are close to the body in the resting state in the absence of DNA. Upon formation of the gyrase heterotetramer, they are released, but maintain their down-position. In an early step of the catalytic cycle of DNA gyrase, binding of a G-segment at the DNA-gate, and possibly a first contact of the DNA with the CTDs, trigger an upward and twisting movement of the CTDs. As a result, the CTDs face away from the GyrA body and are in a position to guide the DNA substrate toward T-segment capture by closure of the N-gate.

MATERIAL AND METHODS

Plasmid constructs and site-directed mutagenesis

The *Bacillus subtilis* gyrA gene was subcloned into the BamHI and XhoI restriction sites of the pACYCDuet-1 vector (Merck Biosciences, Darmstadt, Germany). A TEV protease cleavage site was inserted by site-directed mutagenesis, resulting in a protein of the sequence His_6-P-E-N-L-Y-F-Q|-S2-GyrA. GyrA lacking the CTDs was constructed by subcloning the gyrA gene into the BamHI and HindIII restriction sites of pETDuet-1 (Merck Biosciences), and introducing a stop codon after the codon for amino acid 489. Site-directed mutagenesis

was performed according to the Quikchange protocol (Stratagene, La Jolla, CA, USA).

Protein production and purification

Bacillus subtilis GyrA, GyrA_ΔCTD, GyrA_Y123F and GyrB were produced and purified as described (8,12,19). Hetero-dimeric GyrA containing one cysteine-free mutant [C350L, wildtype-like (8)] and one subunit containing two cysteines for labeling (in addition to the C350L mutation) was produced in *Escherichia coli* BL21(DE3), co-transformed with pACYCDuet-1 (GyrA_C350L, plus two cysteines) and pET-27 b (GyrA_C350L), in auto-induction medium (20) at 30°C for 24 h, and purified via chromatography on Ni^{2+}-NTA sepharose and size-exclusion chromatography. All purification steps were performed at 4°C in buffer A (50 mM Tris/HCl, pH 7.5, 1 M NaCl, 10 mM $MgCl_2$ and 2 mM β-mercaptoethanol). Cells were disrupted in a microfluidizer in Buffer A in the presence of protease inhibitor (Roche) and cell debris was removed by centrifugation. The supernatant was applied to a Ni^{2+}-NTA column (GE Healthcare) equilibrated in Buffer A containing 20 mM imidazole. Bound protein was eluted with Buffer A containing 500 mM imidazole, incubated with TEV protease during overnight dialysis against Buffer A containing 500 mM NaCl (Buffer B), and purified on the Ni^{2+}-NTA column equilibrated in Buffer B and 20 mM imidazole. The flow-through was dialyzed against Buffer B with 300 mM NaCl, concentrated and purified on a calibrated S200 size-exclusion column (GE Healthcare) equilibrated with the same buffer.

GyrA and GyrA_ΔCTD eluted as apparent dimers. Protein concentrations were determined photometrically using the calculated extinction coefficients ε (280 nm) of 42 750 $M^{-1}cm^{-1}$ (GyrA), 41 260 $M^{-1}cm^{-1}$ (GyrA_Y123F), 52 720 $M^{-1}cm^{-1}$ (GyrB), and 25 330 $M^{-1}cm^{-1}$ (GyrA_ΔCTD) [Protparam (21)].

DNA substrates, DNA binding and topoisomerase activity

DNA supercoiling was assayed as described (8,12,19) by incubating 50 nM relaxed pUC18 with 200 nM GyrA and 800 nM GyrB in 50 mM Tris/HCl, pH 7.5, 100 mM KCl and 10 mM $MgCl_2$ in the presence of 2 mM ATP at 37°C, and stopped by the addition of 50 mM EDTA and 5% SDS. Relaxation assays were performed with 15 nM negatively supercoiled pUC18, 200 nM GyrA and 800 nM GyrB without ATP. Products were analyzed on 1.2% agarose gels.

DNA oligonucleotides for the linear dsDNA substrates were from Purimex. The 90 and 110-bp DNAs were from Purimex, or produced by PCR as described (12). All DNA substrates contain the preferred binding site for gyrase (22).

K_d values for DNA substrates were determined in fluorescence anisotropy titrations of 10 nM DNA internally labeled with Alexa546 in 50 mM Tris/HCl, pH 7.5, 100 mM KCl, 10 mM $MgCl_2$, 2 mM β-mercaptoethanol with GyrA, in the absence or presence of 4 μM GyrB as described (8,12) with a Jobin Yvon FluoroMax3 fluorimeter. Fluorescence was excited at 555 nm and detected at 571 nm. Data were analyzed using the solution of the quadratic equation that describes a 1:1 complex formation [Equation (1)]:

$$r = r_0 + \frac{\Delta r_{max}}{[DNA]_{tot}} \cdot \left(\frac{[GyrA]_{tot} + [DNA]_{tot} + K_d}{2} - \sqrt{\left(\frac{[GyrA]_{tot} + [DNA]_{tot} + K_d}{2} \right)^2 - [GyrA]_{tot}[DNA]_{tot}} \right), \quad (1)$$

where r_0 is the anisotropy of free DNA, Δr_{max} is the amplitude, $[GyrA]_{tot}$ is the total GyrA concentration and $[DNA]_{tot}$ is the total DNA concentration.

smFRET experiments

30 μM of GyrA was labeled with 120 μM Alexa488 (donor) and 120 μM Alexa546 (acceptor) in 50 mM Tris/HCl, pH 7.5, 300 mM NaCl, 10 mM $MgCl_2$ containing 1 mM Tris(2-carboxyethyl)phosphine. Labeling efficiencies were determined from absorbance ratios at 495 nm (A_{488}, corrected for A_{546} contributions) and 280 nm (protein, corrected for dye contributions), or at 555 nm (A_{546}) and 280 nm. Statistical labeling leads to a mixed population of D/D–, D/A– and A/D– and A/A– species, as well as the corresponding singly labeled GyrA dimers (D/–, –/D, A/–, –/A). Labeling conditions were optimized to maximize the fraction of species carrying one donor- and one acceptor fluorophore, and to minimize the species carrying only donor moieties. With typical labeling efficiencies of 0.3 (donor) and 0.6 (acceptor) for each cysteine, the fractions of the individual species are as follows: D/D: $0.3 \times 0.3 = 0.09$; D/A, A/D: $2 \times 0.3 \times 0.6 = 0.36$; A/A: $0.6 \times 0.6 = 0.36$; D/–, –/D: $2 \times 0.3 \times (1 - 0.3 - 0.6) = 0.03$; A/–, –/A: $2 \times 0.6 \times (1 - 0.3 - 0.6) = 0.12$. The species carrying only donor generate a 'donor-only' peak that appears at FRET efficiencies <0 due to the correction procedure (see below) that accounts for an acceptor that is not present. Species carrying only an acceptor are excited inefficiently and do not significantly contribute to the FRET histograms.

SmFRET experiments were performed with a home-built confocal microscope at 37°C in 50 mM Tris/HCl, pH 7.5, 100 mM KCl, 10 mM $MgCl_2$ treated with active charcoal with 50 pM fluorescently labeled GyrA (concentration of donor fluorophore) as described (8,12,23). Concentrations were 50 pM (GyrA, donor concentration), 8 μM GyrB, 20 nM pUC18, 500 nM of 110-bp, 90-bp or 60-bp DNA, or 2 μM of 48-bp or 37-bp DNA and 2 mM (ADPNP). Autocorrelation curves were calculated from the donor fluorescence using the Becker&Hickl TCSPC software. Fluorescence bursts above a threshold of 100 photons were included in the analysis. Measured fluorescence intensities were corrected for background, for cross-talk from donor fluorescence into the acceptor channel and vice versa, for different detection efficiencies and quantum yields of donor and acceptor and for direct excitation of the donor as described (23). FRET efficiency correction parameters

and the Förster distance R_0 were determined individually for each construct and both possible dye configurations (D/A, A/D, Supplementary Tables S2–S5) as described (8,12,23). To account for the influence of ligands on the photophysical properties of the dyes, the correction parameters were determined both in the absence of ligands and in the presence of DNA and GyrB (Supplementary Tables S2–S5).

Distance determination and model building

We have previously established that our correction procedure yields corrected FRET efficiencies that reflect correct inter-molecular distances [see Ref. (24) for a detailed description]. Distance histograms were generated by converting the FRET efficiency for each single molecule into an inter-dye distance using the appropriate Förster distance R_0 determined under identical conditions. Distance histograms were described with a single or double Gaussian distribution. Due to the two sets of correction parameters for the D/A– and A/D– species, two distance histograms were obtained for each construct that usually differed by <0.3 nm. For model building, the average distance from both histograms was used (Supplementary Tables S4 and S5). The models for GyrA alone and in the gyrase/DNA complex were obtained by manually placing the structure of the GyrA body [homology model for *B. subtilis* GyrA, created using SWISS-model (25) and the structure of *E. coli* GyrA (26), PDB-ID 1AB4, as a template] and the CTDs [homology model for *B. subtilis* GyrA, created using the structure of *E. coli* GyrA (10), PDB-ID 1ZI0, as a template], such that the experimentally determined inter-dye distances were fulfilled. In the final models, the distances between the thiol groups and the experimentally determined inter-dye distances agree within 0.05 nm. The overall accuracy of the models is limited by the uncertainty of the length of the linkers between thiols and dyes (~0.5 nm).

RESULTS

A strategy toward investigating the movement of the C-terminal domains in *B. subtilis* DNA gyrase

The CTDs of gyrase are required for negative DNA supercoiling, and their deletion converts *E. coli* gyrase into a type II topoisomerase that relaxes DNA in an ATP-dependent fashion (15,27). The CTDs contribute to wrapping of DNA around gyrase in a positive handedness, a prerequisite for strand passage toward negative supercoiling. We first established the critical role of the CTDs for DNA supercoiling by *B. subtilis* gyrase. Gyrase lacking the GyrA CTDs (GyrA_ΔCTD) does not show relaxation of negatively supercoiled DNA in the absence of ATP (Figure 1A), but efficiently relaxes DNA when ATP is present. Gyrase lacking the CTDs is not capable to introduce negative supercoils into DNA, demonstrating that the CTDs are required for the *B. subtilis* gyrase supercoiling activity.

In *E. coli* gyrase, the two CTDs are proposed to flank the sides of the GyrA dimer (17). The distance between the C-terminal residues of the GyrA body is >9 nm [PDB-ID 1AB4 (17)], suggesting that FRET between dyes on different CTDs would be inefficient. Nevertheless, we created cysteine mutants D695C, K570C, K594C and E726C and K594C. K570C and K594C are located close to the N-terminus on opposite faces of blade 2, and D695 and E726 are located on blades 4 and 5 on the distant end of the β-pinwheel fold (Figure 1B). The GyrA dimers were labeled with a mixture of the donor and acceptor fluorophores, yielding a mixture of D/D–, D/A–, A/D– and A/A–labeled protein. These species do not re-equilibrate during handling due to the slow exchange of subunits (8,28). The reaction conditions were optimized such that the predominant species carries one donor and one acceptor, only a minor fraction carries two acceptors or two donors, and negligible fractions carry one acceptor or one donor. Species carrying two acceptors are excited and detected inefficiently and do not appear in relevant amounts in smFRET histograms. Species carrying one or two donors will appear as a 'donor only' peak at apparent FRET efficiencies <0 (see 'Materials and Methods' section). The predominant contribution to FRET histograms thus stems from FRET within GyrA dimers that carry both the donor and the acceptor fluorophore. In-line with the large expected distance between the CTDs, smFRET experiments with the GyrA mutants carrying one label in each CTD revealed low to very low FRET efficiencies (Figure 1C, correction parameters in Supplementary Table S1), confirming that the inter-dye distances are at the limit of the experimentally accessible range. Therefore, we devised an expression/purification system for heterodimeric GyrA containing a cysteine-free (wildtype-like) subunit and a mutant subunit carrying one cysteine on the body of GyrA and a second cysteine on the CTD (see 'Materials and Methods' section). Toward this end, the gene for wild-type GyrA fused to an N-terminal His-tag and the gene coding for the (untagged) double cysteine mutant were introduced into different expression plasmids, and co-transformed into *E. coli* BL21(DE3). Both subunits were co-produced, and heterodimers (as well as wild-type homodimers) were purified using affinity chromatography, and the tag was removed to yield authentic heterodimers (and a fraction of wild-type homodimers that do not carry cysteines and thus are not labeled and not detected in smFRET experiments). Again, subunit exchange during handling and experimentation can be neglected due to the slow exchange kinetics (8). DNA supercoiling activities of the mutants were confirmed (Figure 1A and Supplementary Figure S1).

Localization of the CTDs in GyrA

Cysteines were introduced on the GyrA body (T140C, close to the DNA-gate; E211C, E250C, in the tower domain), at two positions in the CTD (K570C; K594C; Figure 1B and D), and in all possible combinations (GyrA_T140/K570C, GyrA_T140/K594C, GyrA_E211/K570C, GyrA_E211/K594C and GyrA_E250/K570C, GyrA_E250/K594C). Heterodimeric GyrA with one cysteine-free subunit and one subunit containing two cysteines was labeled with AlexaFluor 488 (A488, donor)

and AlexaFluor 546 (A546, acceptor). The supercoiling activities were confirmed for all labeled proteins (Supplementary Figure S1), and smFRET experiments were performed. FRET histograms for all constructs were well-defined, with one predominant distribution of FRET efficiencies, demonstrating that the CTDs adopt a defined conformation in the GyrA dimer (Figure 2). The FRET efficiency is intermediate between the dyes attached to T140C (DNA-gate) and both positions on the CTD (0.3–0.5), and higher (0.6–0.8) if the dye is attached to E211C or E250C (tower domain). Similar high FRET efficiencies of ~0.8 were obtained for two other mutants carrying one dye in the tower domain (T299C, N314C; Supplementary Figure S2).

Corrected FRET efficiencies from smFRET experiments can be used to extract inter-dye distances that reflect true intra-molecular distances (8,23,24,29); see Supplementary Tables S1 and S2 for individual correction parameters and Förster distances for each construct). FRET efficiencies for individual molecules were converted into inter-dye distances, and distance histograms were constructed (Figure 2). Due to the statistical labeling procedure, 50% of the donor/acceptor-labeled proteins carry a donor on the body and an acceptor on the CTD, and the remaining 50% have the inverse orientation of dyes. As the photophysical properties of fluorescent dyes depend on the local chemical environment, the correction parameters and Förster distances for these two forms may differ. Therefore, the parameters were determined individually for both dye configurations (Supplementary Table S2), and FRET histograms were calculated for both sets of parameters (Figure 2). For all double mutants, the two sets of parameters were very similar, and the influence on the determined inter-dye distances was negligible. All distance histograms could be described by a single Gaussian distribution (Figure 2), but showed tailing toward larger inter-dye distances, pointing toward some conformational heterogeneity.

To identify the orientation of the CTDs with respect to the GyrA body, the mean distances of the fitted Gaussian distributions from all FRET experiments (Supplementary Table S4) were used as distance constraints to manually position the residues 570 and 594 of the CTD relative to the labeled residues on the GyrA body (homology-model for *B. subtilis* GyrA, based on the structure of *E. coli* GyrA, see 'Materials and Methods' section, Figure 3A). Together with the low FRET efficiencies between residues on the CTDs across the dimer (Figure 1C), the data are consistent with a downward-facing CTD position, similar to the model originally proposed from SAXS data [(17); see 'Discussion' section).

Formation of the gyrase heterotetramer and DNA binding: complex assembly

We next probed conformational changes in the CTD upon assembly of gyrase and gyrase/DNA complexes. When the gyrase heterotetramer was formed upon the addition of GyrB to GyrA_T140/K594C and GyrA_T140/K570C (Figure 4A and B), the FRET efficiencies decreased. Similarly, FRET efficiency for the GyrA dimer labeled on both CTDs decreased slightly upon gyrase formation. These data are indicative of a larger distance between the CTD and the GyrA body in gyrase, possibly as a consequence of rearrangements at the DNA-gate upon GyrB binding. The addition of negatively supercoiled pUC18 to GyrA led to a broadening of the distribution (Figure 4C), pointing toward conformational flexibility of the CTDs in the GyrA/DNA complex. DNA was bound to GyrA under these conditions, as evidenced from the increased duration of fluorescence bursts, and shifts in the autocorrelation curve due to increased diffusion times (Supplementary Figure S4). For GyrA_T140/K570C and GyrA_K594C, the FRET efficiency of the GyrA/DNA complex was reduced compared to free GyrA, and for GyrA_T140/K594C it was slightly increased. Finally, when GyrB was added to the GyrA/DNA complexes, the FRET efficiencies decreased to ~0 for all constructs (Figure 4D), showing that the CTDs are now in a different position. The same histograms for the gyrase/DNA complex were obtained irrespective of the order of addition of GyrB and DNA. For all constructs, the FRET efficiencies for the gyrase/DNA complexes are different from the FRET efficiency of gyrase alone, demonstrating that the CTDs move upon DNA binding to gyrase. As the DNA-gate of gyrase is in the closed conformation and does not undergo large conformational changes when plasmid DNA binds (8), the changes in FRET efficiencies must reflect movement of the CTDs. FRET histograms in the presence of relaxed DNA gave similar results as in the presence of negatively supercoiled DNA (Figure 6A).

Localization of the CTDs in the gyrase/DNA complex

To gain further insight into the position of the CTDs in the gyrase/DNA complex, we performed smFRET experiments for all constructs in the presence of GyrB and (negatively supercoiled) DNA (Figure 5). While the FRET histograms again appeared unimodal for all constructs, or were very broad, some of the distance distributions were now clearly bimodal. In all of these cases, the predominant species was the one with a higher inter-dye distance. The origin of the second species with a lower inter-dye distance is not clear (see Discussion). For positioning of the CTDs in the gyrase/DNA complex, the mean distances of the distributions with the larger inter-dye distance were used (Supplementary Table S5). These distance constraints locate the two labeled residues in the CTDs in a different position compared to free GyrA and gyrase (Figures 3B, C, and 4B). Together with the loss of FRET between dyes on the CTD across the GyrA dimer (Supplementary Figure S3), the results are consistent with the CTDs of both subunits having swung upward and rotated away (Figure 3C).

Validation of the models for GyrA and gyrase

From the triangulated positions of the two labeled residues in the CTDs, models for GyrA in the absence and gyrase in the presence of DNA can be constructed from homology models of the *B. subtilis* GyrA and CTD

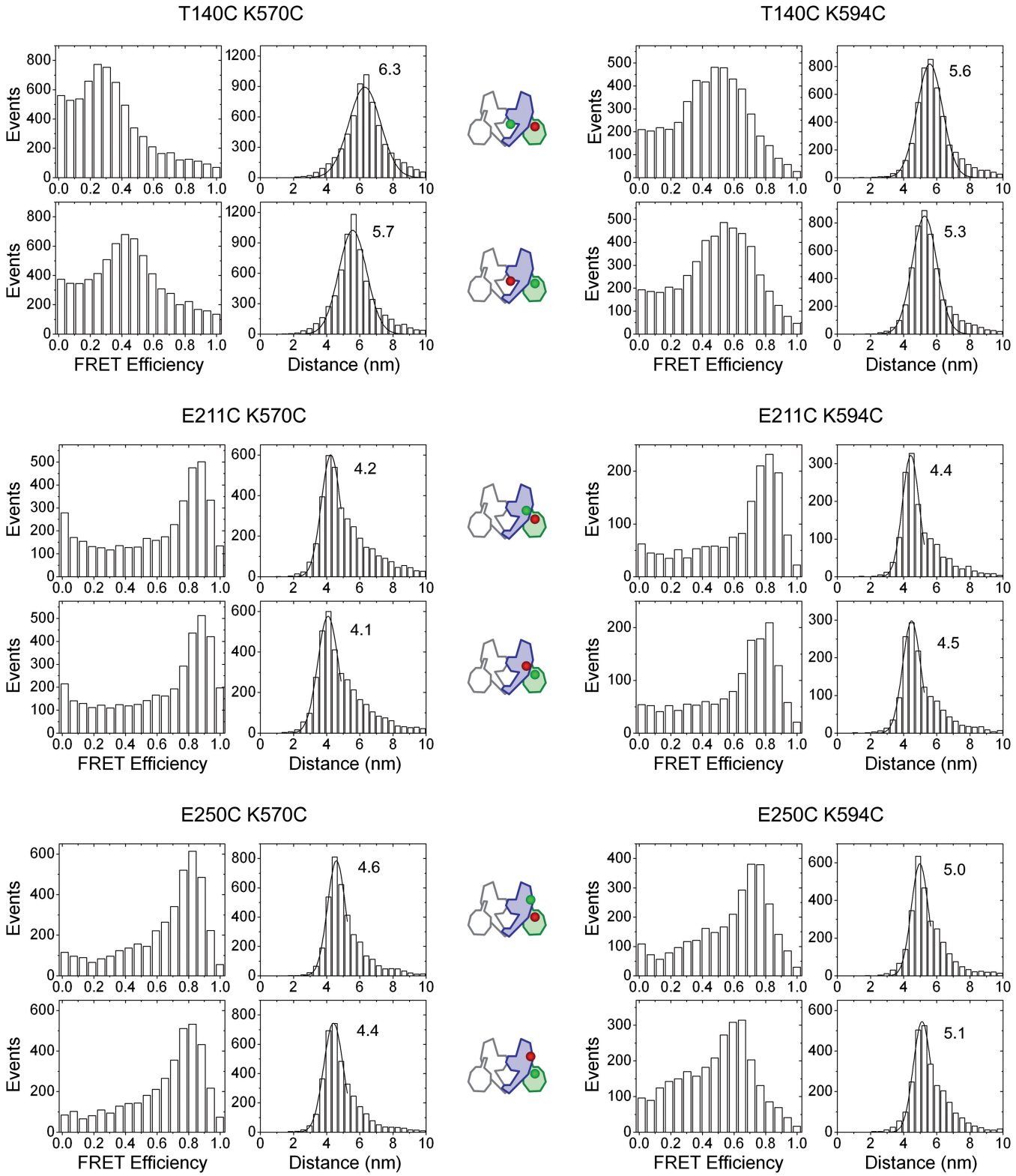

Figure 2. smFRET histograms for donor/acceptor-labeled GyrA in the absence of DNA. smFRET histograms for heterodimeric GyrA containing one cysteine-free subunit and one mutant subunit with one cysteine on the body (T140C close to the DNA-gate, or E211C or E250C in the tower domain) and one cysteine in the CTD (K570C, K594, blade 2). For each donor/acceptor-labeled construct, the FRET histograms (left) and the distance histograms (right) are depicted. Numbers denote the mean distances (in nm) of the Gaussian distribution (line) describing the distance histograms. The upper panel for each construct shows histograms obtained with correction parameters and Förster distances for the donor attached to the GyrA body and the acceptor to the CTD, and the lower panel shows histograms obtained with correction parameters and Förster distances for the inverse orientation (acceptor on GyrA body and donor on CTD). The cartoon indicates the position of the donor (green) and acceptor dye (red). The orientation of the dyes in general has little effect on the determined inter-dye distances. Unimodal FRET distributions are consistent with a defined and symmetric position of the two CTDs.

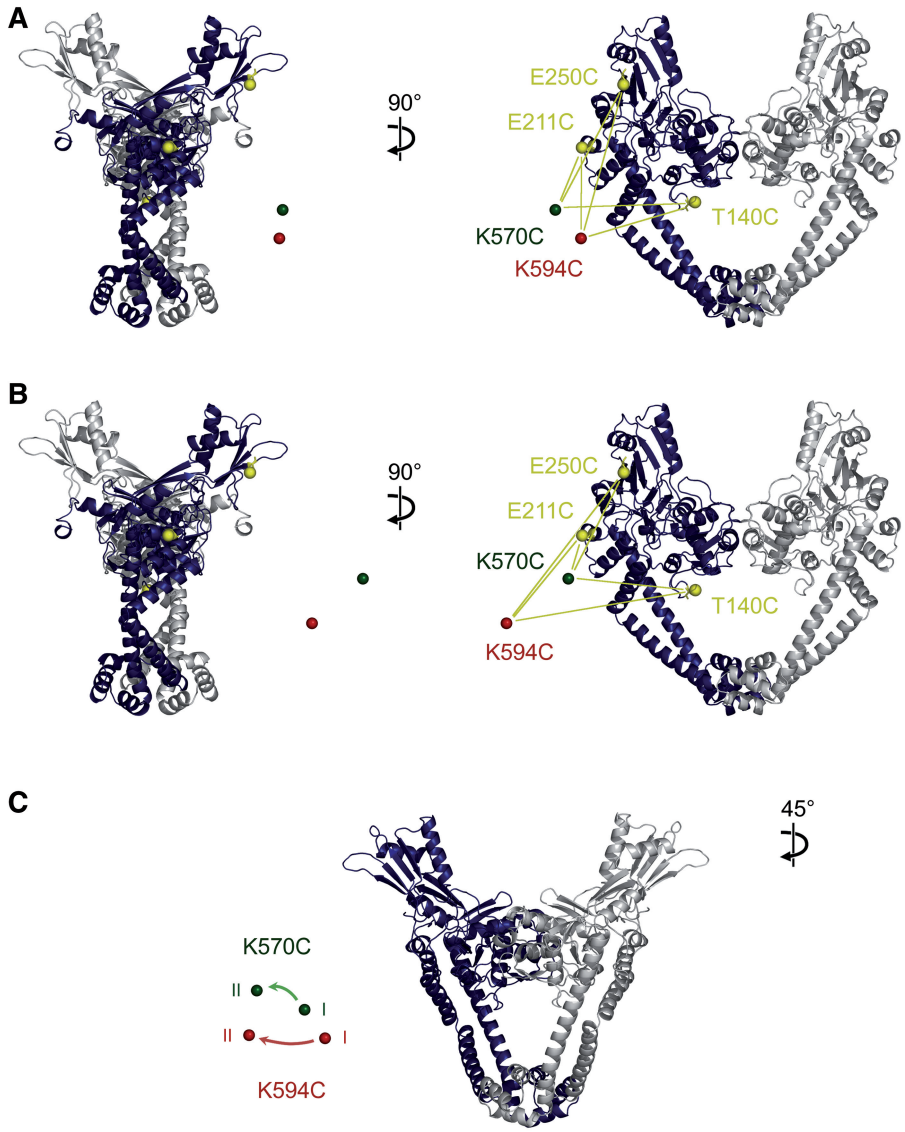

Figure 3. Localization of the CTDs in GyrA and in the gyrase/DNA complex. Reconstruction of the CTD position in the GyrA dimer (**A**) and in the gyrase/DNA complex (**B**) from distance constraints derived from the smFRET experiments (Figure 2, 5). The distances used are the mean of the two distances obtained for D/A or A/D configurations. Spheres indicate the positions of K570C (green) and K594C (red). The distances of the dyes on the CTD increase 0.5–1 nm with respect to E211C and E250C, and 1.5–2.4 nm with respect to T140C in the gyrase/DNA complex, corresponding to an extension of the CTDs from the gyrase body in the presence of DNA (**C**, superposition of A and B, I: positions of K570C (green) and K594C (red) in GyrA, II: positions in the gyrase/DNA complex). The depicted structures are homology models of *B. subtilis* GyrA, generated using the *E. coli* GyrA structure as a template (see 'Materials and Methods' section).

(see 'Materials and Methods' section) that are in agreement with the distance constraints from smFRET experiments (Figure 7). In principle, defining the positions of two reference points leaves the rotation around the joining axis as a remaining degree of freedom. The available conformational space for the CTD in the two states is clearly different (Supplementary Figure S5) and can be narrowed when the FRET efficiencies between dyes on the CTDs across the GyrA dimer (Figure 1C and Supplementary Figure S3), steric clashes with the GyrA body and a likely orientation of the CTD N-terminus toward the C-terminus of the GyrA body are considered. To validate the models (Figure 7), we constructed additional mutants to obtain qualitative distance information between blade 2 and the C-gate. GyrA_N399C/K594C (C-gate/blade 2) shows a FRET efficiency of ~0.1 (Supplementary Figure S2), corresponding to an inter-dye distance of ~8 nm. This value is in good agreement with the distance of 7.8 nm predicted from the model. The FRET efficiency decreases to zero when GyrB and plasmid are added, in-line with an increase in the inter-dye distance. Again, this is consistent with the model that predicts an inter-dye distance of ~10 nm. Obtaining additional FRET constraints is difficult due to the large distances involved. This is illustrated by FRET histograms of GyrA_T408C/D695C, labeled at the distant edge of the CTD (blade 4) and the C-gate: Here, the FRET efficiency was zero both in the absence

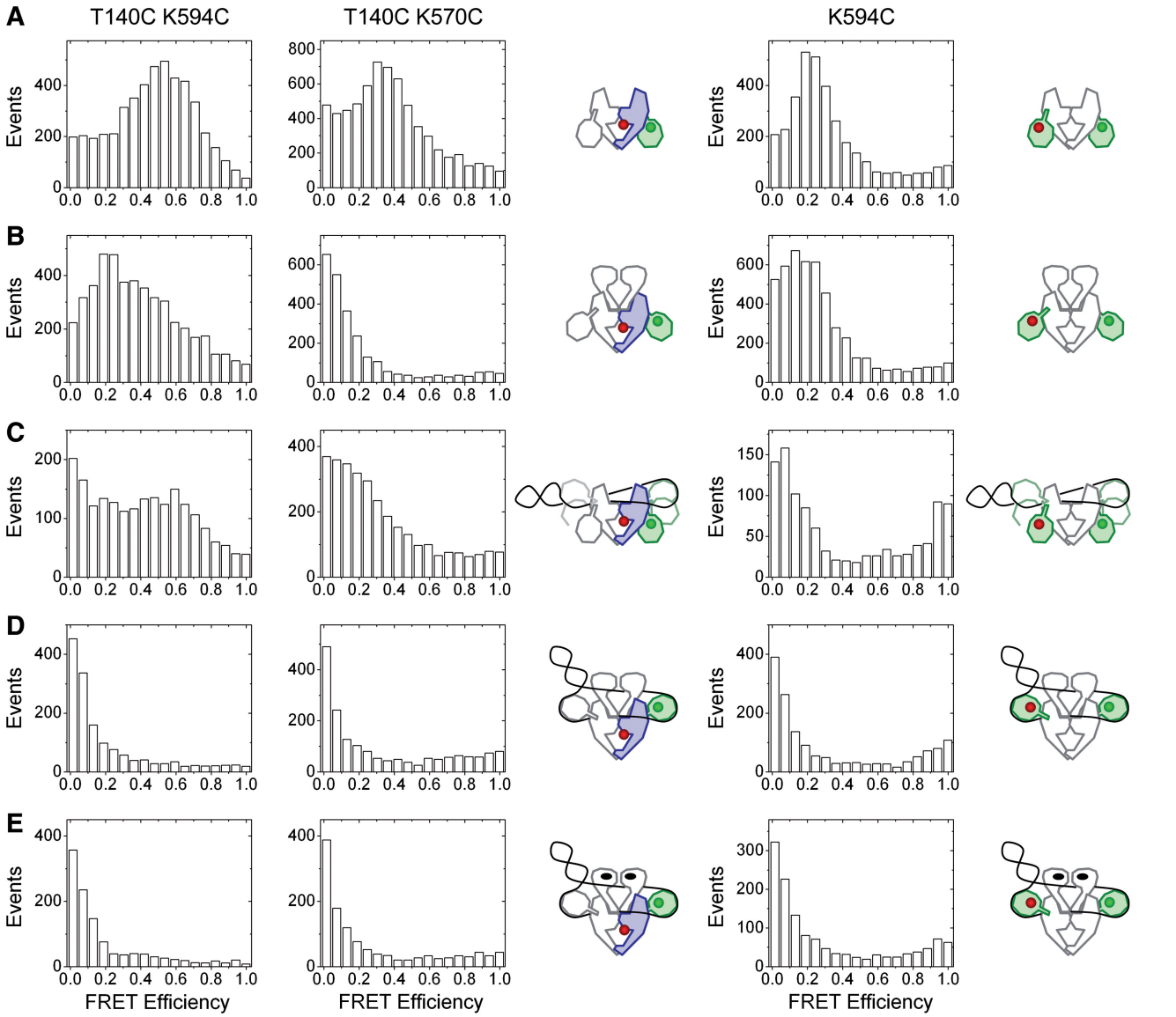

Figure 4. Conformational changes of the CTDs upon complex assembly. smFRET histograms for GyrA_T140/K594C and GyrA_T140/K594C (heterodimers), and GyrA_K594C (homodimer) in the absence of ligands (**A**), in the presence of GyrB (**B**), in the presence of negatively supercoiled plasmid (**C**), in the presence of GyrB and negatively supercoiled plasmid (**D**) and in the presence of GyrB, negatively supercoiled plasmid and ADPNP (added in this order, **E**). The cartoons indicate the components present in each experiment, and the positions of the fluorescent dyes (green and red spheres). A slight change in FRET efficiency indicates a movement of the CTDs further away from the GyrA body upon formation of the A_2B_2 heterotetramer. In the complex of GyrA with plasmid DNA, the histograms are broad, pointing toward flexibility of the CTDs. When DNA binds to gyrase, the FRET efficiency decreases to ~0, consistent with a large conformational change of the CTDs away from the GyrA body. The addition of the nonhydrolyzable nucleotide analog ADPNP that induces a closure of the N-gate does not significantly influence the FRET efficiency and thus the position of the CTDs.

and the presence of GyrB and plasmid (Supplementary Figure S2). Finally, FRET experiments with GyrA_T140C/D695C (DNA-gate/blade 4) place the distant edge of the CTD within 4–6 nm of the DNA-gate in GyrA and in the gyrase/DNA complex, again consistent with the derived models.

Short linear DNA substrates induce the extended GyrA conformation

Binding of negatively supercoiled plasmid to gyrase causes the CTDs to swing upward into a more extended conformation (Figure 3). Binding of relaxed plasmid to GyrA or gyrase elicited the same CTD movement (Figure 6A), indicating that the supercoiling state of the DNA substrate is not important for this conformational change to occur. To test whether wrapping of DNA around the CTDs is required for their upward movement, we tested the effect of 37-bp, 48-bp, 60-bp, 90-bp and 110-bp DNA (Supplementary Figure S6, Ref. 12) on the CTD position. All of these DNAs bind to gyrase, with $K_d < 0.7\,\mu M$. The affinity of gyrase for DNAs is increasing with length, from a K_d of 0.65 μM

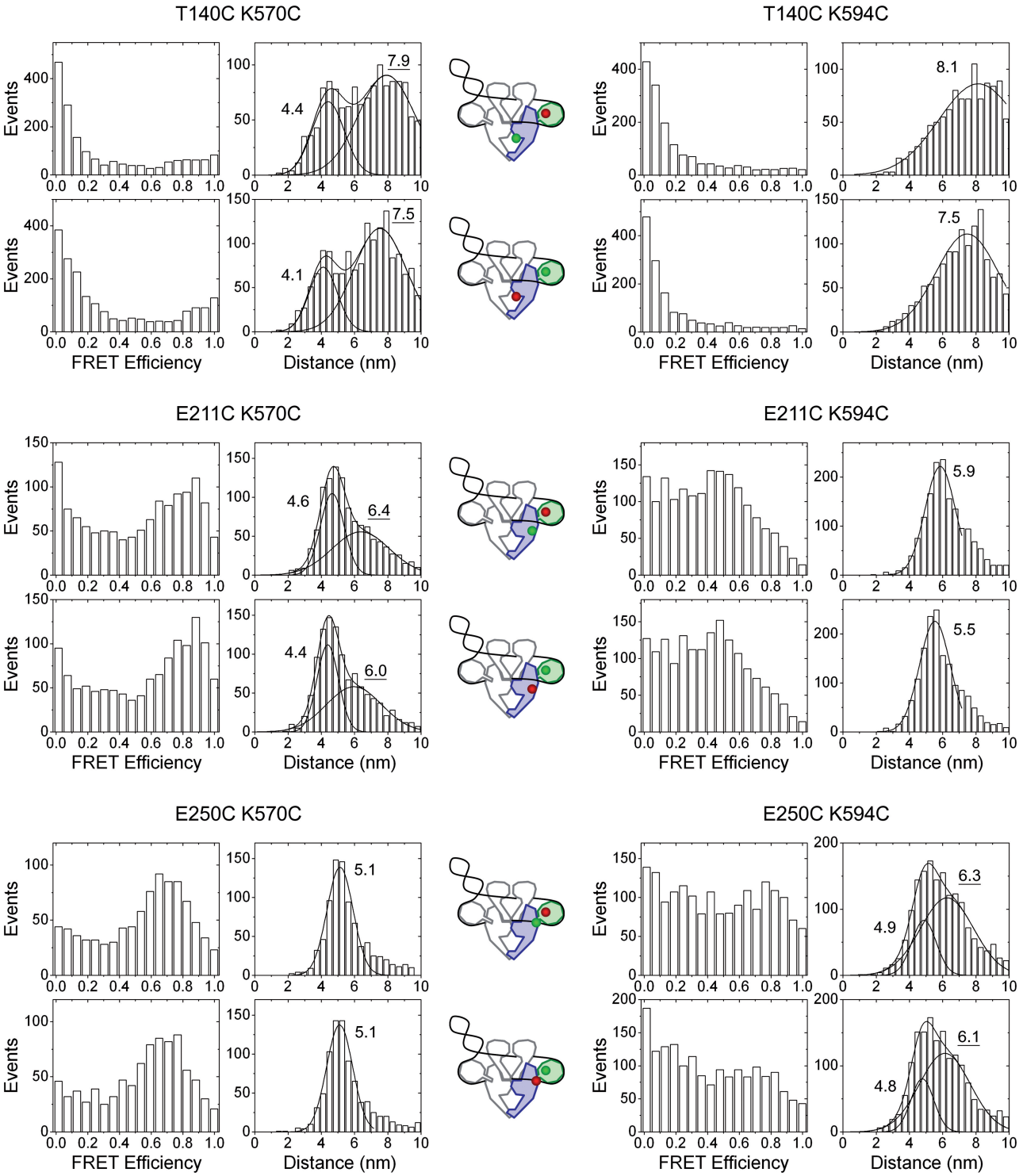

Figure 5. smFRET histograms for the donor/acceptor-labeled gyrase/DNA complex. smFRET histograms for gyrase containing one cysteine-free GyrA subunit and one GyrA mutant subunit with one cysteine on the body (T140C close to the DNA-gate, or E211C or E250C, in the tower domain) and one cysteine in the CTD (K570C, K594, blade 2). For each donor/acceptor-labeled construct, the FRET histograms (left) and the distance histograms (right) are depicted. Numbers denote the mean distances (in nm) of the Gaussian distribution (line) describing the distance histograms. The underlined distance was used for CTD positioning (see 'Materials and Methods' section). The upper panel for each construct shows histograms obtained with correction parameters and Förster distances for the donor attached to the GyrA body and the acceptor to the CTD; the lower panel shows histograms obtained with correction parameters and Förster distances for the inverse orientation (acceptor on GyrA body and donor on CTD). The cartoon indicates the position of the donor (green) and acceptor dye (red). The orientation of the dyes in general has little effect on the determined inter-dye distances. FRET distributions are still unimodal, but distance histograms clearly show bimodal distributions. The origin of the two distributions is not clear (see 'Discussion' section).

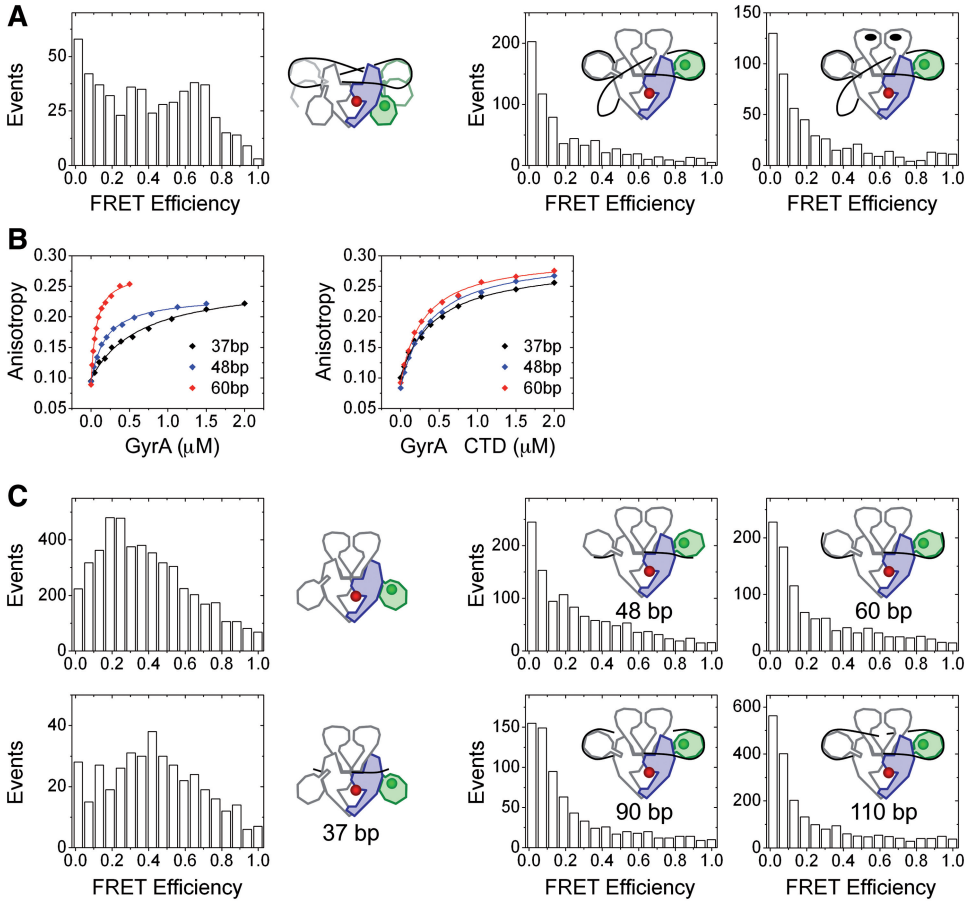

Figure 6. Short linear DNA substrates induce CTD movement. (**A**) smFRET histograms for GyrA_T140C/K594C in the presence of relaxed plasmid, and for gyrase containing one GyrA_T140C/K594C subunit in the presence of relaxed plasmid, and in the presence of relaxed plasmid and ADPNP (added to the gyrase/DNA complex). The cartoons indicate the components present in each experiment, and the positions of the fluorescent dyes (green and red spheres). (**B**) Anisotropy titrations of linear DNA of different lengths with gyrase. The K_d values are 654 nM (37 bp), 190 nM (48 bp), and 63 nM (60 bp). (B) Anisotropy titrations with gyrase lacking the CTDs. The K_d values are 460 nM (37 bp), 380 nM (48 bp) and 298 nM (60 bp). (**C**) smFRET histograms for gyrase containing one GyrA_T140C/K594C subunit with DNA substrates of different lengths. A low FRET efficiency of ~0 is observed for the 48-bp, 60-bp, 90-bp, and 110-bp DNA, indicative of the upward position of the CTDs. In contrast, the FRET efficiency remains at ~0.4 in complex with 37-bp DNA, corresponding to the down-conformation of the CTDs in the resting state. The cartoons indicate the components present in each experiment, and the positions of the fluorescent dyes (green and red spheres).

(37 bp) to 0.06 μM (60 bp, Figure 6B), and increases further for 90- and 110-bp DNA (12), in-line with more extensive interactions with gyrase being formed. Surprisingly, binding of the 48-bp DNA and all longer DNAs induced the conformational change of the GyrA CTDs (Figure 6C). In contrast, the 37-bp DNA did not affect the CTD position. From crystal structures of topoisomerase II in complex with DNA (30), the length of a gate-DNA (not contacting CTDs) can be estimated to comprise 30–40 bp. Consequently, a 37-bp DNA is too short to form interactions with the CTDs, whereas a 48-bp DNA already extends from the DNA-binding site at the DNA-gate and will establish contacts with the CTDs. The smFRET data thus indicate that the upward motion of the CTDs results from first contacts of the bound DNA with the CTDs, but does not require complete wrapping of the DNA around the CTD perimeter.

To clarify whether the linear DNAs bind to the DNA-gate only or also contact the CTDs, we measured the corresponding K_d values of gyrase/DNA complexes with GyrA_ΔCTD (Figure 6B). K_d values were still slightly decreasing with DNA length (0.46 μM, 0.38 μM and 0.30 μM, respectively), but to a far lesser extent. The affinities of the full-length enzyme were 2- and 5-fold higher for the 48-bp and 60 bp-DNAs, respectively, when the CTDs were present, indicating that these DNAs contact the CTDs, with the 60-bp DNA engaging in more extensive contacts with the CTDs than the 48 bp. In contrast, the K_d value for the 37-bp DNA complex decreased 1.4-fold when the CTDs were deleted, suggesting that the CTDs do not positively contribute to binding of this DNA, and possibly reflecting a small inhibitory effect of the CTDs on binding of the 37-bp DNA to the DNA-gate. Altogether, our findings thus demonstrate that the conformational change of the CTDs is induced by DNAs that are sufficiently long to bind at the DNA-gate and to establish first contacts with the CTD via flanking regions.

Conformational changes during the supercoiling cycle: order of events

The conformational change of the CTDs upon DNA binding to GyrA already occurs with short linear DNAs (>48 bp), and to similar extents with relaxed and negatively supercoiled DNA, suggesting that the upward movement of the CTDs is not coupled to complete DNA wrapping, but may only require first contacts of the DNA bound at the DNA-gate with the CTDs. In contrast, complete wrapping of DNA around the CTDs induces a narrowing of the N-gate, preparing it for complete closure upon ATP binding, and for T-segment capture (12). N-gate narrowing requires the presence of the CTDs and does not occur in a cleavage-deficient gyrase mutant (12). To relate the conformational change of the CTDs to other events in the catalytic cycle of gyrase, we tested if a cleavage-deficient gyrase mutant responds to DNA binding by an upward movement of the CTDs. SmFRET histograms of cleavage-deficient gyrase were indistinguishable from wild-type histograms in the absence, and similar in the presence of DNA (Supplementary Figure S7), indicating that the conformational change does not require DNA cleavage and may even precede cleavage in the catalytic cycle of gyrase. Hence, the upward movement of the CTDs is an early event in the catalytic cycle of gyrase.

We next tested the effect of ADPNP-induced N-gate closure on the position of the CTDs. SmFRET histograms of gyrase (GyrA_T140/K570C) in the presence of ADPNP, and thus with a closed N-gate, were similar to the histograms for gyrase in the absence of ADPNP, demonstrating that N-gate closure *per se* does not affect the CTD conformation (Supplementary Figure S4). When plasmid was added to gyrase (GyrA_T140/K570C and GyrA_T140/K594C) with a closed N-gate, the FRET efficiency decreased, corresponding to the extended CTD conformation (Supplementary Figure S4). The increase in diffusion time of the complex confirms that DNA is bound (Supplementary Figure S4). This observation demonstrates that a T-segment is not required for movement of the CTDs and suggests that interactions of the plasmid at the DNA-gate and first contacts of flanking regions with the CTDs are sufficient to trigger the observed release of the CTDs to their upward position. When a gyrase/DNA complex was preformed, and the N-gate was subsequently closed by the addition of ADPNP, the FRET efficiency remained low (Figures 4E and 6A), characteristic of the extended conformation. Thus, the CTDs remain in their upward position when the N-gate closes, and return to their resting position with a higher FRET efficiency later in the supercoiling cycle.

DISCUSSION

The data in this study are consistent with the CTDs being in a downward conformation, below the active site, in the resting state of gyrase. DNA binding at the DNA-gate and first contacts of flanking regions of the DNA with the CTDs cause the CTDs to swing upward and sideways, resulting in a more extended conformation of GyrA (Figure 7A). The conformational change of the CTDs upon DNA binding has been suggested previously (17), but so far not observed experimentally. The localization of the CTDs in gyrase in the absence of DNA is in general agreement with a previous SAXS model, although the CTD is rotated and displaced with respect to the SAXS model (Figure 7B). In the model for GyrA in the gyrase/DNA complex that satisfies the experimental distance constraints, blades 1, 4, 5 and 6 of the CTDs are accessible and face away from the GyrA body, consistent with their proposed role in DNA binding (10). A recent SAXS study of gyrase in the presence of DNA has put forward a model with the CTDs in a downward orientation closer to the C-gate of gyrase (18). Our smFRET results argue against such a conformation in the DNA-bound form of gyrase for linear DNAs as well as for relaxed and negatively supercoiled plasmid DNA. While the reasons for the discrepancy are not clear, the smFRET experiments are performed under conditions of supercoiling (8), and should reflect on-pathway intermediates during the catalytic cycle. The upward movement of the CTDs upon DNA binding is independent of G-segment cleavage, placing it at an early stage of the gyrase catalytic cycle.

Binding of the G-segment at the DNA-gate and first contacts of the DNA with the CTD are sufficient to trigger the upward movement of the CTDs. What causes the upward movement of the CTDs upon DNA binding? Possible explanations are (i) contacts of residues on the body (or the CTD) with DNA that compete for interactions between the GyrA body and the CTD stabilizing the downward-facing conformation, (ii) a re-organization of the DNA-gate upon DNA binding, altering the conformation of the linker between the GyrA body and the CTDs, causing CTD release, or (iii) direct interactions of the CTDs with GyrB that stabilize the extended GyrA conformation. Our smFRET model places the CTDs with an appreciable distance from the gyrase body both in the downward- and the upward-facing orientation, rendering direct interactions between the CTDs and GyrA or GyrB unlikely. This notion is supported by the observation that the CTDs do not need to be covalently attached to the GyrA body to promote negative supercoiling (9). On the other hand, the DNA-gate is formed by GyrA and GyrB subunits (31), and binding of GyrB to GyrA already causes a partial release of the CTDs, supporting that a re-organization of the DNA-gate can be transmitted to the CTDs. Similarly, local conformational changes of gyrase at the DNA-gate upon binding of the G-segment may prepare CTD movement, and first interactions of the adjacent DNA regions with the CTDs will then trigger the conformational change. The CTDs are required for distortion of DNA at the DNA-gate (12). The movement of the CTDs upon DNA binding is possible in cleavage-deficient gyrase that is not capable to distort the bound G-segment (8), but it may have different consequences when distortion of the G-segment is possible. GyrB is required for distortion of the G-segment (8) and for the upward movement of the CTDs upon G-segment binding, further linking these events. If the DNA flanking the G-segment is long enough to be wrapped around the CTDs completely, narrowing of the N-gate will follow

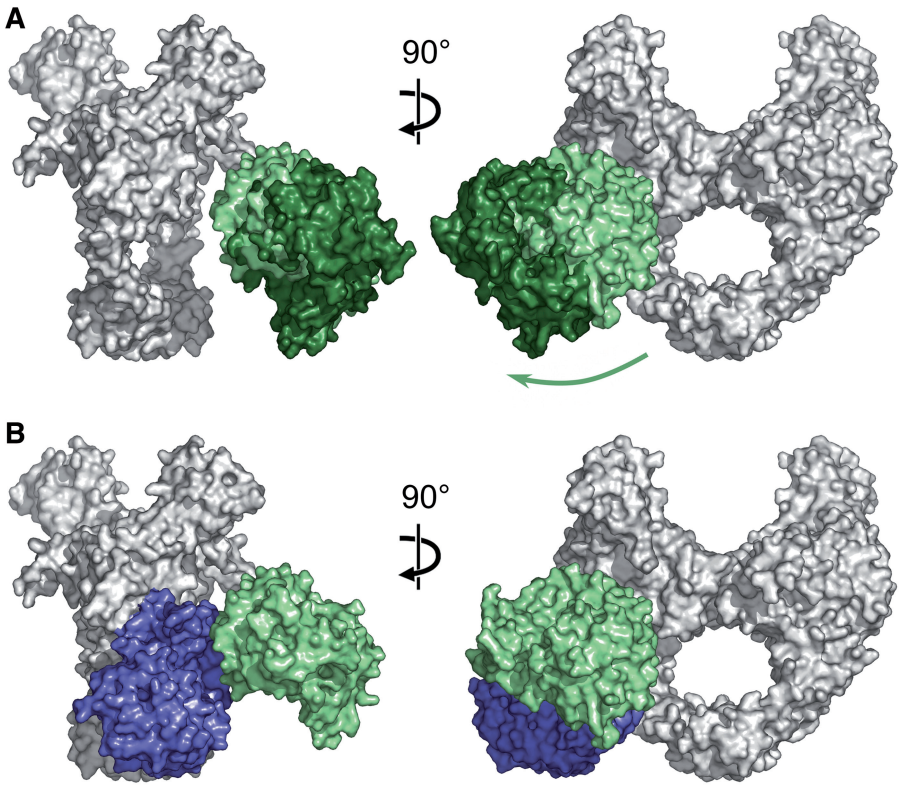

Figure 7. Model for CTD conformations in the absence and presence of DNA, and comparison to previously suggested models. (**A**) Structural model of GyrA body (gray) and the CTDs in the GyrA dimer (light green) and in gyrase bound to DNA (dark green) in side (left) and front view (right). CTDs are depicted with residues K570 and K594 overlapping with the corresponding reference points derived from smFRET data and the N-terminus facing the GyrA body C-terminus (see the main text). The green arrow indicates the CTD movement upon binding of GyrB and DNA to GyrA. (**B**) Comparison of GyrA models from smFRET (this work, CTD in light green) and SAXS data [(17) CTD in blue] depicted from the side (left) and front (right). The CTD are in downward-facing positions in both models, but closer to the GyrA body in the SAXS model. The depicted models for *B. subtilis* GyrA (body) and the *B. subtilis* CTD are homology models, generated using the *E. coli* GyrA and CTD structures as a template (see 'Materials and Methods' section).

(12), and the geometry of the bound DNA will lead to the positioning of a T-segment between the GyrB arms. N-gate closure then completes T-segment capture and poises gyrase for strand passage. Overall, the CTD movement thus helps guide a T-segment into the upper cavity.

A net loss of wrapping upon ADPNP binding to the N-gate of gyrase (32) has been interpreted as a release of the CTDs from the DNA when the N-gate closes and captures a T-segment, rendering them available for grabbing a subsequent T-segment for the next round of supercoiling. However, the lack of movement of the CTDs upon N-gate closure argues against a release of the CTDs in this step and instead suggests that they return to the downward position at later stages. Nevertheless, smFRET data point toward a fixation of the CTDs when ADPNP binds and indicate that the interaction of the CTDs with the DNAs may be altered when the N-gate closes. Strikingly, FRET experiments in the absence of DNA are consistent with symmetric conformations of gyrase, whereas in the gyrase/DNA complexes, bimodal distributions of inter-dye distances point toward the presence of asymmetric conformations, that may reflect gyrase with one CTD in the up-, the other in the down conformation. Although gyrase contains two CTDs that wrap DNA adjacent to the G-segment, clearly only one T-segment can be presented to the upper cavity. The two conformers we observe in the presence of DNA may be first direct experimental support for a previously proposed hand-over-hand mechanism, with one CTD in the upward position presenting a T-segment, and the second in the down position, waiting for its turn to present a T-segment in the next cycle. However, the populations of the two observed conformers are not equal, as the mechanism would predict. Future experiments will have to address the existence of asymmetric gyrase/DNA complexes, and the question as to when in the catalytic cycle the symmetry may be broken.

Implications for the supercoiling cycle

Binding of DNA to the DNA-gate of gyrase initiates the supercoiling cycle. We have shown here that binding of DNA at the DNA-gate of gyrase and first contacts with the CTDs cause an upward movement of the CTDs, leading to an extended GyrA conformation (Figure 8). In a tightly coupled process, the G-segment is then distorted, flanking regions are wrapped around the CTDs and the G-segment is cleaved. N-gate narrowing upon complete wrapping of DNA around the CTDs positions a T-segment between the GyrB arms, either due to the

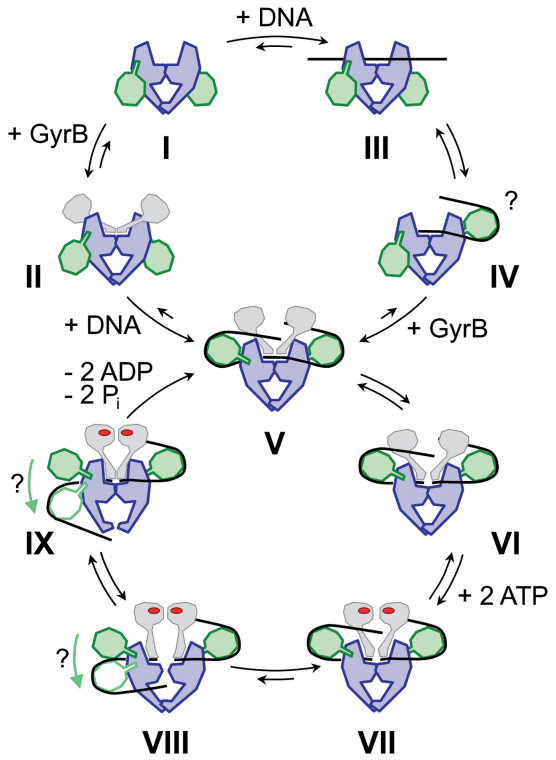

Figure 8. Model for CTD conformation in the catalytic cycle of gyrase. Model of the CTD movements during the assembly of gyrase and DNA (I–V) and the supercoiling reaction cycle (V–IX). GyrA body, GyrA CTDs and GyrB are shown in blue, green and gray, respectively; DNA is depicted as a black line, and nucleotide is shown in red. (I) CTDs are located close to the GyrA body in the free enzyme. (II) Upon binding of GyrB, they slightly move away from the core. (III) Presumably, initial binding of DNA to GyrA takes place at the DNA-gate. (IV) Contacts of the DNA with the CTDs result in the extension of the CTDs (IV). (V) The active enzyme complex with an extended conformation of the CTDs is formed if GyrB is present. (V, VI) The active enzyme complex can cleave DNA (VI). VI exhibits a slightly more extended CTD conformation than V. (VII) Nucleotide binding induces ATPase gate closure, but does not cause a significant CTD. (VIII, IX) hypothetical CTD movements upon transfer of T-DNA segment through the open DNA-gate (VIII) and C-gate (IX). The CTD bound to the T-segment may guide or follow the transfer movement and transiently swing toward the C-gate, predicting asymmetry with respect to the position of the two CTDs in gyrase. The bimodal distributions observed for the gyrase/DNA complex may point toward the existence of such asymmetric conformers. The supercoiling cycle is completed by hydrolysis of ATP and release of ADP and P_i (V).

intrinsic geometry of the bound DNA, or due to the geometry enforced by the CTDs. The narrowing of the N-gate is coupled to the unlocking of the DNA-gate. At this stage of the catalytic cycle, the CTDs remain in their upward position. ATP binding to the GyrB subunits promotes N-gate closure, traps the T-segment, triggers opening of the DNA-gate and pushes the T-segment through the gap in the G-segment at the DNA-gate. The CTDs are in the upward position when ADPNP has bound, but may be released to help capture a T-segment for subsequent cycles upon ATP hydrolysis and N-gate re-opening. Our results illustrate how a hierarchical, coordinated and tightly coupled sequence of conformational changes leads to T-segment capture and strand passage in the catalytic cycle of DNA gyrase. Understanding the conformational changes coupling ATP-hydrolysis to DNA supercoiling may open up avenues for developing novel and improved gyrase inhibitors.

SUPPLEMENTARY DATA

Supplementary Data are available at NAR Online.

ACKNOWLEDGEMENTS

We thank Airat Gubaev for discussions, and Ines Hertel, Andreas Schmidt and Diana Blank for excellent technical assistance.

FUNDING

The VolkswagenStiftung; the Swiss National Science Foundation; the NCCR Nanoscale Sciences. Funding for open access charge: University of Basel.

Conflict of interest statement. None declared.

REFERENCES

1. Gellert,M., Mizuuchi,K., O'Dea,M.H. and Nash,H.A. (1976) DNA gyrase: an enzyme that introduces superhelical turns into DNA. *Proc. Natl Acad. Sci. USA*, **73**, 3872–3876.
2. Williams,N.L. and Maxwell,A. (1999) Probing the two-gate mechanism of DNA gyrase using cysteine cross-linking. *Biochemistry*, **38**, 13502–13511.
3. Williams,N.L. and Maxwell,A. (1999) Locking the DNA gate of DNA gyrase: investigating the effects on DNA cleavage and ATP hydrolysis. *Biochemistry*, **38**, 14157–14164.
4. Kampranis,S.C., Bates,A.D. and Maxwell,A. (1999) A model for the mechanism of strand passage by DNA gyrase. *Proc. Natl Acad. Sci. USA*, **96**, 8414–8419.
5. Williams,N.L., Howells,A.J. and Maxwell,A. (2001) Locking the ATP-operated clamp of DNA gyrase: probing the mechanism of strand passage. *J. Mol. Biol.*, **306**, 969–984.
6. Wigley,D.B., Davies,G.J., Dodson,E.J., Maxwell,A. and Dodson,G. (1991) Crystal structure of an N-terminal fragment of the DNA gyrase B protein. *Nature*, **351**, 624–629.
7. Tingey,A.P. and Maxwell,A. (1996) Probing the role of the ATP-operated clamp in the strand-passage reaction of DNA gyrase. *Nucleic Acids Res.*, **24**, 4868–4873.
8. Gubaev,A., Hilbert,M. and Klostermeier,D. (2009) The DNA Gate of *Bacillus subtilis* gyrase is predominantly in the closed conformation during the DNA supercoiling reaction. *Proc. Natl Acad. Sci. USA*, **106**, 13278–13283.
9. Reece,R.J. and Maxwell,A. (1991) The C-terminal domain of the *Escherichia coli* DNA gyrase A subunit is a DNA-binding protein. *Nucleic Acids Res.*, **19**, 1399–1405.
10. Ruthenburg,A.J., Graybosch,D.M., Huetsch,J.C. and Verdine,G.L. (2005) A superhelical spiral in the Escherichia coli DNA gyrase A C-terminal domain imparts unidirectional supercoiling bias. *J. Biol. Chem.*, **280**, 26177–26184.
11. Corbett,K.D., Shultzaberger,R.K. and Berger,J.M. (2004) The C-terminal domain of DNA gyrase A adopts a DNA-bending beta-pinwheel fold. *Proc. Natl Acad. Sci. USA*, **101**, 7293–7298.
12. Gubaev,A. and Klostermeier,D. (2011) DNA-induced narrowing of the gyrase N-gate coordinates T-segment capture and strand passage. *Proc. Natl Acad. Sci. USA*, in press.
13. Tretter,E.M., Lerman,J.C. and Berger,J.M. A naturally chimeric type IIA topoisomerase in *Aquifex aeolicus* highlights an evolutionary path for the emergence of functional paralogs. *Proc. Natl. Acad. Sci. USA*, **107**, 22055–22059.

14. Ward,D. and Newton,A. (1997) Requirement of topoisomerase IV parC and parE genes for cell cycle progression and developmental regulation in Caulobacter crescentus. *Mol. Microbiol.*, **26**, 897–910.
15. Kramlinger,V.M. and Hiasa,H. (2006) The "GyrA-box" is required for the ability of DNA gyrase to wrap DNA and catalyze the supercoiling reaction. *J. Biol. Chem.*, **281**, 3738–3742.
16. Kirchhausen,T., Wang,J.C. and Harrison,S.C. (1985) DNA gyrase and its complexes with DNA: direct observation by electron microscopy. *Cell*, **41**, 933–943.
17. Costenaro,L., Grossmann,J.G., Ebel,C. and Maxwell,A. (2005) Small-angle X-ray scattering reveals the solution structure of the full-length DNA gyrase a subunit. *Structure*, **13**, 287–296.
18. Baker,N.M., Weigand,S., Maar-Mathias,S. and Mondragon,A. (2011) Solution structures of DNA-bound gyrase. *Nucleic Acids Res.*, **39**, 755–766.
19. Gottler,T. and Klostermeier,D. (2007) Dissection of the nucleotide cycle of *B. subtilis* DNA gyrase and its modulation by DNA. *J. Mol. Biol.*, **367**, 1392–1404.
20. Studier,F.W. (2005) Protein production by auto-induction in high density shaking cultures. *Protein Expr. Purif.*, **41**, 207–234.
21. Gasteiger,E., Hoogland,C., Gattiker,A., Duvaud,S., Wilkins,M.R., Appel,R.D. and Bairoch,A. (2005) Protein identification and analysis tools on the ExPASy server. In Walker,J.M. (ed.), *The Proteomics Protocols Handbook*. Humana Press, New York, USA, pp. 571–607.
22. Bashkirov,V.I. and Zvingila,D.J. (1991) Sequence specificity of *Bacillus subtilis* DNA gyrase *in vivo*. *Genetica*, **85**, 3–12.
23. Theissen,B., Karow,A.R., Kohler,J., Gubaev,A. and Klostermeier,D. (2008) Cooperative binding of ATP and RNA induces a closed conformation in a DEAD box RNA helicase. *Proc. Natl Acad. Sci. USA*, **105**, 548–553.
24. Hilbert,M., Kebbel,F., Gubaev,A. and Klostermeier,D. (2010) eIF4G stimulates the activity of the DEAD box protein eIF4A by a conformational guidance mechanism. *Nucleic Acids Res.*, **39**, 2260–2270.
25. Schwede,T., Kopp,J., Guex,N. and Peitsch,M.C. (2003) SWISS-MODEL: an automated protein homology-modeling server. *Nucleic Acids Res.*, **31**, 3381–3385.
26. Morais Cabral,J.H., Jackson,A.P., Smith,C.V., Shikotra,N., Maxwell,A. and Liddington,R.C. (1997) Crystal structure of the breakage-reunion domain of DNA gyrase. *Nature*, **388**, 903–906.
27. Kampranis,S.C. and Maxwell,A. (1996) Conversion of DNA gyrase into a conventional type II topoisomerase. *Proc. Natl Acad. Sci. USA*, **93**, 14416–14421.
28. Tennyson,R.B. and Lindsley,J.E. (1997) Type II DNA topoisomerase from *Saccharomyces cerevisiae* is a stable dimer. *Biochemistry*, **36**, 6107–6114.
29. Karow,A.R. and Klostermeier,D. (2010) A structural model for the DEAD box helicase YxiN in solution: localization of the RNA-binding domain. *J. Mol. Biol.*, **402**, 629–637.
30. Dong,K.C. and Berger,J.M. (2007) Structural basis for gate-DNA recognition and bending by type IIA topoisomerases. *Nature*, **450**, 1201–1205.
31. Schoeffler,A.J., May,A.P. and Berger,J.M. (2010) A domain insertion in *Escherichia coli* GyrB adopts a novel fold that plays a critical role in gyrase function. *Nucleic Acids Res.*, **38**, 7830–7844.
32. Heddle,J.G., Mitelheiser,S., Maxwell,A. and Thomson,N.H. (2004) Nucleotide binding to DNA gyrase causes loss of DNA wrap. *J. Mol. Biol.*, **337**, 597–610.